ACCSCIENCE PUBLISHING

Materials Science in Additive Manufacturing

ORIGINAL RESEARCH ARTICLE

3D-Printed disposable nozzles for cost-efficient extrusion-based 3D bioprinting

Hamed I. Albalawi[1,2,3], Zainab N. Khan[1], Ranim H. Rawas[1,2,3], Alexander U. Valle-Pérez[1,2,3], Sherin Abdelrahman[1,2,3], and Charlotte A. E. Hauser[1,2,3]*

[1]Laboratory for Nanomedicine, Division of Biological and Environmental Science and Engineering (BESE), King Abdullah University for Science and Technology, Thuwal 23955-6900, Saudi Arabia

[2]Computational Bioscience Research Center (CBRC), King Abdullah University of Science and Technology, Thuwal 23955, Saudi Arabia

[3]Red Sea Research Center, King Abdullah University of Science and Technology, Thuwal 23955, Saudi Arabia

Abstract

3D bioprinting has significantly impacted tissue engineering with its capability to create intricate structures with complex geometries that were difficult to replicate through traditional manufacturing techniques. Extrusion-based 3D bioprinting methods tend to be limited when creating complex structures using bioinks of low viscosity. However, the capacity for creating multi-material structures that have distinct properties could be unlocked through the mixture of two solutions before extrusion. This could be used to generate architectures with varying levels of stiffness and hydrophobicity, which could be utilized for regenerative medicine applications. Moreover, it allows for combining proteins and other biological materials in a single 3D-bioprinted structure. This paper presents a standardized fabrication method of disposable nozzle connectors (DNC) for 3D bioprinting with hydrogel-based materials. This method entails 3D printing connectors with dual inlets and a single outlet to mix the material internally. The connectors are compatible with conventional Luer lock needles, offering an efficient solution for nozzle replacement. IVZK (Ac-Ile-Val-Cha-Lys-NH2) peptide-based hydrogel materials were used as a bioink with the 3D-printed DNCs. Extrusion-based 3D bioprinting was employed to print shapes of varying complexities, demonstrating potential in achieving high print resolution, shape fidelity, and biocompatibility. Post-printing of human neonatal dermal fibroblasts, cell viability, proliferation, and metabolic activity were observed, which demonstrated the effectiveness of the proposed design and process for 3D bioprinting using low-viscosity bioinks.

Keywords: 3D bioprinting; Nozzle connecter; Extrusion-based 3D printing; 3D-printed nozzle; Disposable nozzles

***Corresponding author:**
Charlotte A. E. Hauser
(charlotte.hauser@kaust.edu.sa)

Citation: Albalawi HI, Khan ZN, Rawas RH, *et al.*, 2023, 3D-Printed disposable nozzles for cost-efficient extrusion-based 3D bioprinting. *Mater Sci Add Manuf,* 2(1): 52. https://doi.org/10.36922/msam.52

Received: February 15, 2023

Accepted: March 6, 2023

Published Online: March 21, 2023

1. Introduction

Three-dimensional (3D) printing is a manufacturing technique that can produce 3D objects in a layer-by-layer fashion using computer-aided design (CAD). It has been adopted by many industries, including education, aerospace, transportation, biomedicine, and healthcare[1-4]. More recently, 3D printing has been applied for sustainable and

eco-friendly coral restoration[5-7]. One of the main branches of 3D printing technology is 3D bioprinting, which fabricates cell-based tissue constructs for tissue engineering and regenerative medicine[8]. 3D bioprinting is revolutionizing tissue engineering with its ability to create cell-integrated structures with complex geometries, which were previously unattainable with traditional manufacturing methods. Nevertheless, 3D bioprinting technology is still confined by certain constraints. One significant constraint is related to the 3D printing of structures similar to the complex hierarchical structure of natural tissues[9]. Various 3D printing technologies are used today in 3D bioprinting, such as extrusion-based and vat polymerization.

Vat polymerization is one of the 3D printing technologies used in fabricating tissue engineering scaffolds, relying on a light source, and polymerization reaction to cure a photocurable bio-based resin[10]. The materials utilized in vat polymerization for 3D bioprinting are usually photocurable resins and photocrosslinkable hydrogels. Using photocrosslinkable hydrogel in vat polymerization can enable cell encapsulation and replicate the extracellular matrix found in native tissue[11]. Elomaa *et al.*[12] developed a bioactive photocrosslinkable resin derived from a decellularized small intestine submucosa for vat polymerization-based 3D bioprinting. The developed bioactive resin offers a printable material that acts as a suitable medium for fabricating a complex 3D tissue model. However, vat polymerization application in fabricating cell-based scaffolds is limited due to the high ultraviolet (UV) exposure intensity and the cytotoxicity effect of polymerization reaction[13]. Consequently, this technique is limited to fabricating acellular scaffolds that can only be seeded with cells post-printing. Therefore, other 3D printing technologies can provide the necessary freedom in fabricating and mimicking 3D tissue models.

Extrusion-based 3D printing is a technique that is widely used in fabricating cell-based scaffolds in the 3D bioprinting process[14,15]. More recently, there has been an interest to integrate smart and intelligent biomaterials with 3D printing technology[16]. A pressure-based or mechanical feeder is used to extrude material through a nozzle[17]. While this layer-by-layer approach facilitates fabrication, it has limitations with low-viscosity materials when creating complex structures due to resolution constraints and instantaneous gelation properties of soft matter bioinks, such as peptide hydrogels. On the other hand, high-viscosity biomaterials produce a high shear force, resulting in a high degree of cell destruction during extrusion. Often, cross-linking methods are used to reduce the viscosity of biomaterials and improve cell viability[18]. However, alternative solutions could be developed by maximizing the instantaneous gelation property of low-viscosity bioinks to reduce shear force in the nozzle and eliminate post-printing crosslinking procedures. For instance, several low-viscosity bioinks for 3D bioprinting and cell culture have been developed[19,20]. Incorporating the mixing of multiple solutions before extrusion offers the potential for creating structures with various properties. Multi-material bioinks consisting of solutions such as proteins, hydrogels, and cells can create a more realistic 3D-bioprinted structure that could be advantageous for tissue engineering applications.

In multiple studies, extrusion-based 3D bioprinting and customized 3D-printed parts have been combined to create tissue scaffolds with desired characteristics. For instance, Khan *et al.*[21] combined vat polymerization and extrusion-based 3D bioprinting to create a complex human-like ear structure. Likewise, Abdelrahman *et al.* implemented a hybrid 3D bioprinting and vat polymerization approach for the modeling of Parkinson's disease using dopaminergic neurons[22]. Furthermore, Scott *et al.*[23] have 3D-printed a nozzle to enable multi-material 3D bioprinting using an extrusion-based system. This allows the nozzle to mix multiple solutions and create a multi-material structure. Through further research, researchers have looked into the advantages of merging various 3D printing techniques for utilization in different applications[6,24]. It has been demonstrated that the convergence of 3D printing techniques can upgrade 3D bioprinters and exploit material characteristics for enhanced printability and resolution.

Herein, we propose a design and fabrication process for disposable nozzle connectors (DNC) to accelerate the nozzle-making process for low-viscosity bioinks. It was curated to allow instantaneous mixing of three solutions for the formulation of a continuous bioink thread embedded with cells. The connectors were designed to easily fit into standard Luer lock needle tips, making them versatile and compatible with a wide range of mixing requirements and bioink viscosities. Our design parameters were set for the material characteristics of peptide bioinks, and several tests were performed to assess workability and printability. With a thorough evaluation, the developed DNC proved to be cost-effective, reproducible, and highly practical for standardization.

2. Methods

With the assistance of vat polymerization technology, several DNCs were designed to suit peptide bioink requirements and 3D-printed with varied final diameters and mixing regions. An ideal design was selected based on ease of flow and effective gelation. The 3D-printed DNCs were assembled with Luer lock needle tips to create fully functional nozzles with multiple inlets and a

single outlet, as shown in Figure 1. A range of constructs were then 3D-bioprinted through a microfluidic syringe pump-based extrusion system with peptide-based and live cells. To determine the feasibility of the proposed connectors, an evaluation of the 3D-bioprinted construct was conducted in terms of gelation continuity, printability, biocompatibility, and shape fidelity. The methods applied for designing, fabricating, assembling, and evaluating DNCs for cellular 3D bioprinting with peptide bioinks are detailed in the following.

2.1. Designing DNC

To ensure uniformity, the connectors were designed using the NX CAD software with millimeter precision. Considering the desired needle tip diameter and angle, the connector was designed to fit into a Luer lock needle tip. By design, the two inlets of the connector merge into one channel considering the volume of the two solutions flowing inside the connector. This was done to reduce any material clogging before extrusion. The mixing region length was taken from a previous study to complement the characteristic requirements of our peptide hydrogels for 3D bioprinting[25-27]. This can be modified based on the characteristics of the desired printing materials. The DNC was designed with an additional holder for the cells inlet to enable extruding cells at the tip of the nozzle. An ideal design was narrowed down based on ease of flow through the mixing region while maintaining an inlet angle closest to 90° angle.

2.2. 3D printing connectors using vat polymerization

Connectors were 3D-printed using FormLabs 3B 3D printer in the recommended settings for the white polymer resin. Before 3D printing, the design files were converted to the STL format and then processed with PreForm software to prepare for slicing. The materials were chosen, and the model configuration took place during this process. Following the printing process, the 3D-printed model was washed with isopropanol for 30 min and then cured at a temperature of 40°C for 60 min using the Form Washer and Form Cure post-processing devices.

2.3. Parameter optimization for 3D bioprinting

For seamless material extrusion with the DNC, optimization experiments were run with an in-house developed robotic 3D bioprinter to evaluate gelation, printability, and shape fidelity. For all experiments, 13 mg/mL IVZK (Ac-Ile-Val-Cha-Lys-NH2) peptide and ×7 phosphate-buffered saline (PBS) were used. The cells inlet was pumped with ×1 PBS for acellular simulation tests. A gelation continuity test was conducted by running the microfluidic pumps connected to the DNC at a range of flow rates for peptide and PBS, to determine optimal gelation parameters. A g-code file for a continuous 5-segment line was used to trace any clumps or clogs and gelation time was recorded.

To assess printability, a six-layer semi-filled cube was 3D-printed with the DNC. Based on the gelation continuity test, the optimized flow rates were set to 55 µL/min, 20 µL/min, and 20 µL/min for peptide, PBS, and the cells inlet, respectively. Constructs were evaluated for print shape, consistent formation of bioink thread, and continuous layer deposition.

2.4. Creating acellular 3D-printed scaffolds

Finally, to evaluate the shape fidelity of bioprinted constructs, acellular samples were printed and observed for print resolution and mechanical stiffness. The DNC was mounted on the robotic 3D bioprinter to print hollow cylinders of 10 × 10 × 13 mm^3 and grid structures of 20 mm^2. To enhance flow for longer periods of time, automated time-dependent pumping was exploited by programming the microfluidic pumps with alternating square wave flow profiles. Based on the optimized parameters reported previously, the square wave flow profile for the peptide hydrogel solution was set to a range of 50 – 55 µL/min with a 75% duty cycle and a period of 115 s. For the PBS, the square wave flow profile was set to a range of 15 – 20 µL/min with a 25% duty cycle and a period of 115 s[28].

2.5. 3D cell culture

The biocompatibility of peptide hydrogel biomaterials of IVZK peptide was tested with human neonatal dermal fibroblasts (HDFn). HDFn was cultured in a 3D-bioprinted construct with self-assembling ultra-short IVZK peptide-based hydrogels. An optimal gelation concentration of the IVZK peptide (13 mg/mL) was used. Purified and lyophilized peptide powder was sterilized using a UV light for 30 min before each experiment.

HDFn was obtained from Thermo Fisher Scientific, and cell suspensions were used after seven passages for every experiment. First, 1 mL of Dulbecco's modified eagle medium (DMEM, ×1) was supplemented with 4.5 g/L glucose, 1-glucamine, sodium pyruvate, 10% fetal bovine serum (FBS), and 1% penicillin/streptavidin (10,000 units/mL). After adding cells to the growth medium, the mixture was centrifuged for 5 min (250 ×*g*), at room temperature, to remove the DMSO storage buffer from the stock solution. Then, cells were cultured in 75 mL of growth medium within cell-treated flasks and incubated for 2 days at 37°C. After incubation, the cells were viewed under a microscope to determine their confluency. Then, the growth medium was removed and approximately 5 mL

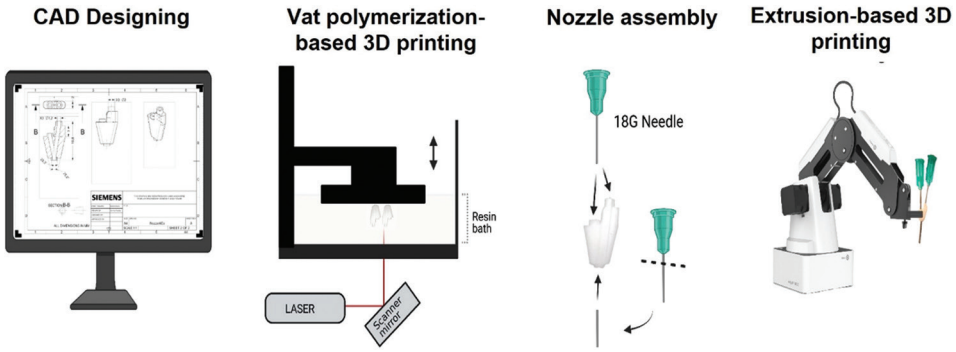

Figure 1. A schematic view of the fabrication process, including CAD designing, 3D printing of DNCs using vat polymerization, DNC nozzle assembly, and extrusion-based 3D bioprinting using the assembled nozzle.
CAD: Computer-aided design; 3D: Three-dimensional; DNC: Disposable nozzle connectors.

of 0.05% trypsin-ethylenediaminetetraacetic acid (×1) was added to the cells to detach them from the surface of the flask. The flask was then incubated at 37°C for 5 min. After the incubation period, the cells were examined under a microscope to confirm detachment. Finally, the solution was transferred into a clean 50-mL centrifuge tube with 10-mL of fresh DMEM (×1). The addition of DMEM (×1) inactivated the trypsin. Then, the cell suspension was centrifuged as described before, and the supernatant was removed. Following this, ×2 PBS was added to the cell pellet to achieve a final cell concentration of 3 million/mL with gentle mixing. The cell suspension with a volume of 0.5 mL was prepared and loaded into the cells inlet pump for bioprinting the 3D constructs.

2.6. 3D Bioprinting of cellular constructs

The robotic 3D bioprinter was mounted with a sterilized disposable nozzle and prepared for 3D bioprinting. Initially, IVZK peptide (13 mg/mL) and ×7 PBS were loaded in Pump 1 and Pump 2 and set to a flow rate range of 50 – 55 µL/min and 15 – 20 µL/min, respectively. Pump 3 was loaded with ×1 PBS and a volume of 0.5 mL HDFn suspension. A six-layer cube with dimensions of 10 × 10 × 2 mm was loaded as g-code and 3D-bioprinted.

2.7. Cell viability testing

The viability of the cellular 3D constructs was examined using the Live/Dead Viability/Cytotoxicity Kit (ThermoFisher, USA). Here, calcein acetoxymethyl ester (Calcein-AM) was used to detect viable cells and ethidium homodimer-I (EthD-I) was used to detect dead cells. DMEM (×1) media was removed from the 3D constructs before the contents of the kit were added. Then, a staining solution of 2 µM calcein-AM and 4 µM of EthD-1 were dissolved in ×1 PBS and the solution was added to the 3D constructs and incubated for 30 min at room temperature. After the incubation period, stained cells were imaged with an EVOS microscope. The viability of HDFn was assessed after 1 and 3 days.

2.8. Cell proliferation assessment

The CellTiter-Glo® luminescent 3D cell viability assay was used to determine the proliferation rate of cells in 3D peptide constructs. An ATP bioluminescence assay works by detecting the presence of living cells in the sample through a bioluminescent signal from metabolically active cells. Dead cells do not produce such a signal since they are not metabolically active. The intensity of the signal is directly proportional to the amount of ATP present in a cell. A volume of the CellTiter-Glo® 3D reagent equivalent to that of the cell culture medium was added to a Petri dish and thoroughly mixed for 5 min, followed by an incubation period of 25 min at room temperature. The bioluminescent signals were read using a plate reader (PHERAstar FS, Germany). The metabolic activity of HDFn was evaluated after 1 and 3 days.

The robotic 3D bioprinter was programmed to deposit bioink and cells into a 96-well plate. This was achieved by mapping the wells in a teach-and-playback approach and setting point-to-point (PTP) positions. The same parameters were used as those optimized for 3D bioprinting. Flow rates of peptide, PBS, and cells were set to 330 µL/min, 120 µL/min, and 120 µL/min, respectively, and they were deposited in each well for 10 s to achieve a volume of 90 µl/well.

2.9. Cytoskeleton staining

Rhodamine phalloidin (Invitrogen, ThermoFisher, USA) was used to stain F-Actin (ex/em ~540 nm/~565 nm) in HDFn. First, culture media was removed; then, the cells were fixed using 4% methanol-free formaldehyde (Thermofisher, USA) for 30 min. The cells were then washed with ×1 PBS after discarding the fixation solution. Subsequently, the cells were incubated for 5 min in a pre-chilled cytoskeleton buffer containing 3 mM $MgCl_2$, 300 mM sucrose, and 0.5%

Triton X-100 in PBS. The cells were then incubated for 30 min at room temperature, in a blocking buffer containing 5% FBS, 0.1% Tween-20, and 0.02% sodium azide in ×1 PBS. Rhodamine-phalloidin (1:40 in ×1 PBS) was added to each well after discarding the blocking buffer. The cells were incubated for 1 h at room temperature. The cells were then washed with ×1 PBS and incubated for 5 min with 4′,6-diamidino-2-phenylindole (DAPI) and sterile water (1:2000, volume/volume). Images were obtained using an EVOS microscope with ×4 and ×10 magnification using absorption and emission parameters. Assessment of the cells' morphology was performed after 1 and 3 days.

3. Results and discussion

This study highlights the apparent advantages of a DNC extrusion system in terms of cost-effectiveness and rapid fabrication time. The use of resins for fabrication makes it extremely simple to modify, fabricate, and replace nozzles as needed without disrupting experiments. In addition, using a vat polymerization-based fabrication method ensures precision and reproducibility, which ensures consistent 3D bioprinting results compared to the inevitable variations in handmade nozzles.

3.1. Design and fabrication of DNC

The connectors were designed to be compatible with standard Luer lock needle tips, where the 18G needle, equivalent to 1.2 mm outer diameter, was used for both inlets and the outlet of the DNC. Furthermore, the two inlets were designed with an angle so that they merge into one outlet, as illustrated in Figure 2A. The minimal angle of the inlet needle placement reduces the possibility of clogging. The design used in this study included an external cell inlet holder used to extrude cells at the nozzle tip (Figure 2B, top). This enabled the deposition of cells into the construct after the gelation process occurred within the DNC mixing region. The DNC illustrated in Figure 2B (bottom) is for printing an acellular peptide-based scaffold.

The DNC STL files were printed with FormLabs 3B using the suggested FormLabs White Resin settings. To eradicate any residual resin, the connectors were post-processed using isopropanol. Subsequently, two 18G needles were inserted into the two inlets, and another 18G needle was cut and sanded to be inserted into the outlet. The needle assembly into the connector was done before the curing process to ensure a sealed fit. Due to the slight shrinkage of the printed models during the curing process, a tight fit between the connectors and needles was created. To finalize the assembly of the nozzle, an 18G needle was inserted into the DNC side holder for the cell's inlet (Figure 2C). The cumulative time taken for printing and curing a batch of 5 DNCs was estimated to be around 3 h.

3.2. Parameter optimization for 3D bioprinting

After fabricating the DNC, several parameters needed to be optimized to establish compatibility with peptide bioinks and our robotic 3D bioprinter. These included flow rate profiles, peptide and PBS concentration, and printing speed. Performance was evaluated by observing gelation continuity, printability, shape fidelity, and biocompatibility.

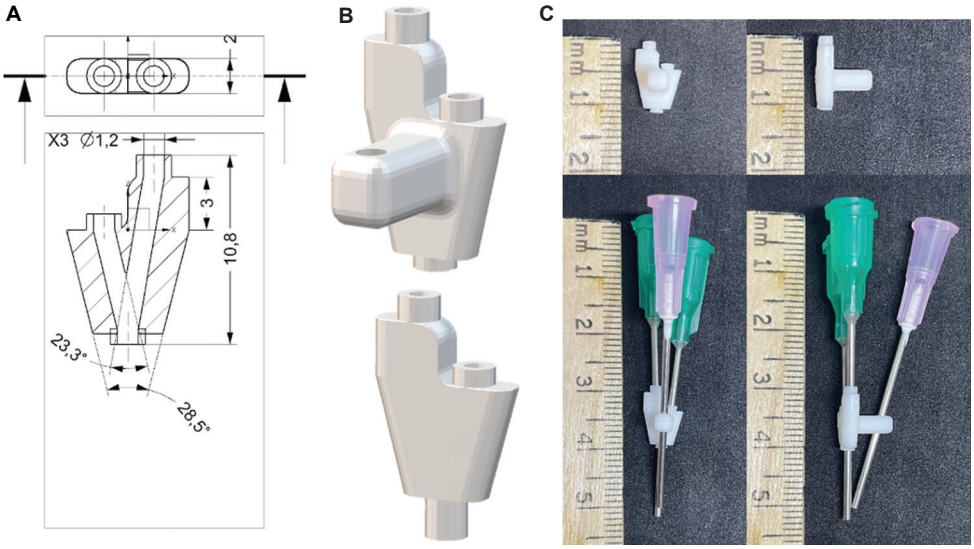

Figure 2. A visual representation of the DNC and the fabrication procedure of the nozzle. (A) A draft drawing showing the dimensions of the DNC and a cross-sectional view of the inlets and the outlet of the DNC, all in mm. (B) A CAD model of the two DNCs with and without the cell inlet holder. (C) The 3D-printed DNC with the needle assembly.
CAD: Computer-aided design; 3D: Three-dimensional; DNC: Disposable nozzle connectors.

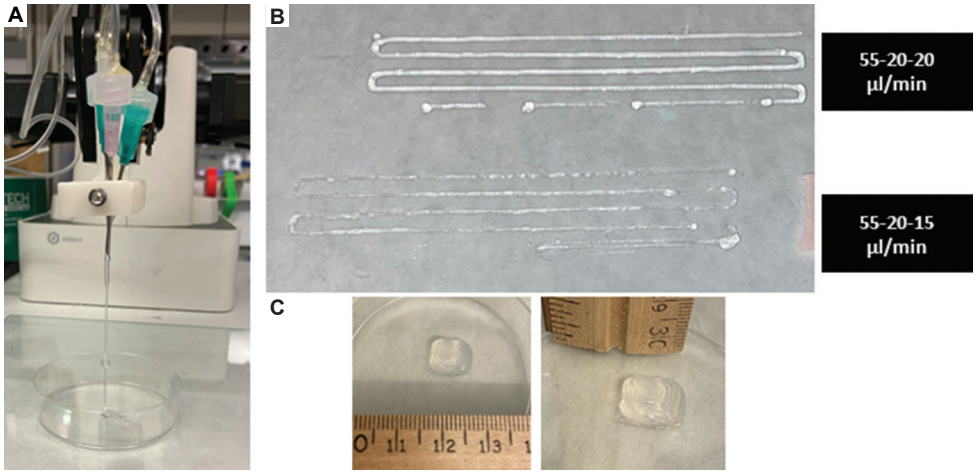

Figure 3. Gelation continuity tests of DNC. (A) Continuous extrusion of peptide bioink thread showing gelation and stiffness. (B) Extrusion of continuous five-segment line at different flow rates to optimize bioink formation. (C) Six-layer cubical constructs showing printability and layer deposition, top view, and side view.
DNC: Disposable nozzle connectors.

In terms of gelation continuity, the best flow rate profile was found to be 55 µL/min, 20 µL/min, and 20 µL/min for the peptide hydrogel, ×7 PBS, and ×1 PBS inlets, respectively. Different flow profiles were tested by printing a continuous 5-segment line, which visibly indicated the period of flow before clumps were formed from over-gelation. A visible thread of gel was also extruded and displayed gel continuity and stiffness, a prime indicator for printability (Figure 3A). Gelation time for the formation of a stable bioink thread was found to be approximately 81 s, which was relatively faster than homemade nozzles. Hence, the optimal flow rates were set according to these observations to be used for further printability assessments (Figure 3B). It was observed that lower flow rates resulted in insufficient flow, which was expected given the mixing region ratio. The gelation therein needed to be accelerated by increasing the overall flow to 95 µL/min.

A six-layer semi-filled cube of dimensions 10 × 10 × 2 mm was 3D-printed using the DNC. Based on the gelation continuity test, the optimized flow rates were set to 55 µL/min, 20 µL/min, and 20 µL/min for the three inlets of peptide, ×7 PBS, and ×1 PBS, respectively. The cubical shape was found to be well maintained with defined lines (Figure 3C, Cube). No clumps or clogs were observed during printing – A key marker of the nozzle performance through consistent formation of bioink thread. In addition, the construct layers piled up smoothly without any sagging, which also indicated continuous layer deposition. For further verification, the peptide flow rate was increased to 60 µL/min for another construct, but results showed lower printing resolution due to several clumps, most likely due to the slightly accelerated gelation.

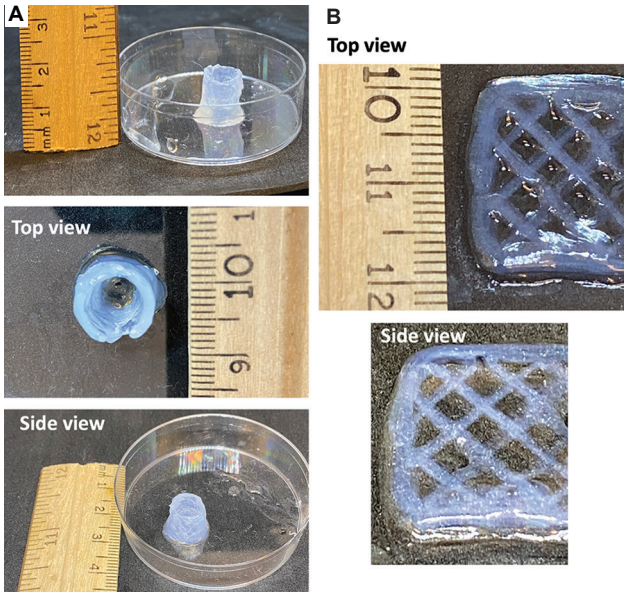

Figure 4. 3D printing of peptide-based acellular constructs with DNC. Different levels of shape complexity were selected: Hollow cylinder 10 × 10 × 13 mm^3 (A), and fine grid 20 mm^2 (B).
3D: Three-dimensional; DNC: Disposable nozzle connectors.

3.3. 3D printing shape fidelity and resolution

To test the DNC, several acellular constructs with different levels of complexity were printed. In addition, automated square wave flow profiles were programmed for the microfluidic pumps to enable smoother flow for longer periods. This was found to ease printing considerably, allowing for 20-min prints without flow interruptions or the need for user intervention to manually alter flow rates. First, a hollow cylinder of 10 × 10 × 13 mm^3 was printed (Figure 4A). This highlighted the layer-by-layer

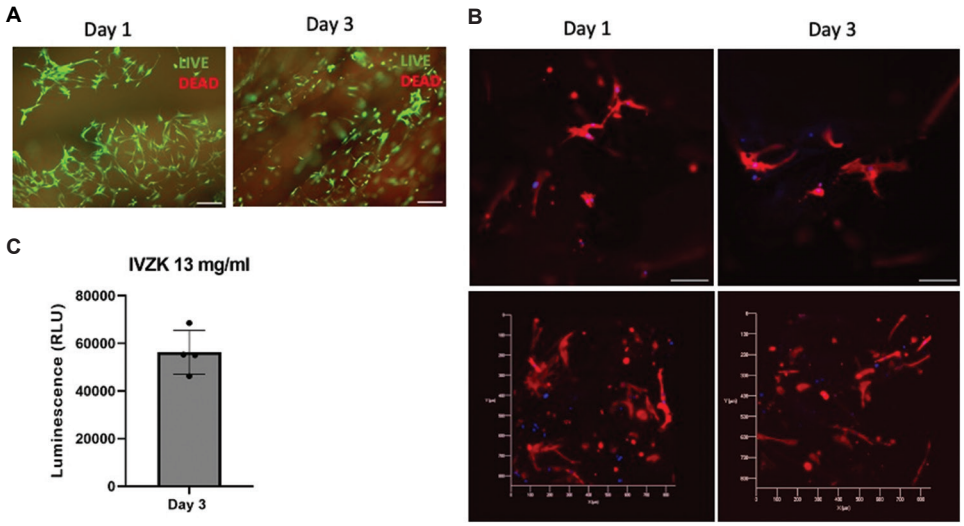

Figure 5. Biocompatibility assays of human neonatal dermal fibroblasts (HDFn) in three-dimensional (3D) IVZK peptide hydrogels constructs were tested for both days 1 and 3 to determine their growth rate and viability. (A) Cells stained with Calcein-AM (green: Live cells) and ethidium homodimer-1 (red: Dead cells). (B) Immunofluorescence staining of the cell nucleus and cytoskeleton protein F-actin. (red: F-actin; blue: nucleus). (C) Finally, the cell viability in 3D constructs of IVZK peptide hydrogel for up to 3 days was tested.

thread deposition for the biomanufacturing of taller constructs. In this case, a continuous thread was formed during printing, suggesting that the interaction design of the nozzle connector avoids clogging. Finally, fine grid squares of 20 mm^2 were 3D-printed to evaluate shape fidelity and print resolution. Figure 4B shows fine threads formed in different layers. According to these results, the DNC shows promising potential to be used as a nozzle connector for peptide-based 3D bioprinting since it enables continuous hydrogel thread extrusion and forms 3D structures with good resolution. Further, in this paper, the integration of cells for 3D bioprinting with DNC is presented.

3.4. 3D cell culture and biocompatibility studies

To assess the cytocompatibility of cells growing in 3D constructs, HDFn was cultured within IVZK peptide hydrogels in 3D constructs. Cell viability, metabolic activity, and morphology assays were performed after 1 and 3 days following bioprinting. HDFn proliferation was evaluated through quantitation of ATP production in metabolically active cells. More live cells growing at a faster rate indicated better biocompatibility of the peptide hydrogels. As shown in Figure 5C, the HDFn viability was good with a percentage of total cells and a growth rate of about >80%. The cell viability was higher after day 3 than, it was on day 1, indicating successful growth and cell division, as confirmed by the ATP assay and live/dead assay results (Figure 5A and C). Cytoskeleton staining was performed to further evaluate the biocompatibility of HDFns in 3D IVZK hydrogels in terms of morphology and interaction of the cells with the material. As illustrated in Figure 5B, the morphology of the HDFn indicated the presence of F-actin filaments, which provide HDFn with mechanical support. Based on these results, we can conclude that HDFn favors the IVZK hydrogel materials, as evidenced by results of the cytotoxicity assays.

4. Conclusions

Beginning from an established point in the field of 3D bioprinting, we provide here a standardized fabrication method of nozzles for 3D bioprinting with hydrogel-based materials to improve reliability of generated data, which will steer the field in a much more standard direction, eventually making it more advanced. This method involves printing connectors with two inlets and an outlet, enabling the material to be mixed within. In addition, these connectors are designed to suit the standard medical needles in the market, allowing the connectors to be used universally, and making them optimal candidates for various mixing requirements and bioink viscosities. Moreover, IVZK peptide-based hydrogel materials possess highly promising properties, making them excellent choices for tissue engineering. The effectiveness of these peptide building blocks has been employed to be compatible with different cell lines such as HDFn. By evaluating the DNC with peptide-based bioinks, 3D constructs were printed with good print resolution, shape fidelity, and mechanical stability, confirming the performance of the DNC in continuous gelation. By taking advantage of the DNC's ability to combine two solutions and incorporate cells during extrusion, we were able to

form 3D-bioprinted structures. The results suggest that HDFn is well suited for the IVZK hydrogel materials post-printing, as demonstrated by cytotoxicity tests, which confirms the biocompatibility of the DNC in 3D bioprinting. We propose the DNC as a solid alternative to the fabrication of handmade nozzles for 3D bioprinting by taking full advantage of rapid prototyping and ensuring standardization and reproducibility.

Acknowledgments

The authors would like to acknowledge Kowther Kahin for her dedicated work in nozzle design, which inspired this work, Noofa Hammad for her technical support on the robotic 3D bioprinter, and Aris Konstantinidis for his support in conducting the experiments.

Funding

This work was financially supported by King Abdullah University of Science and Technology (KAUST).

Conflicts of interest

There are no conflicts of interest to declare.

Author contributions

Conceptualization: Hamed I. Albalawi, Charlotte A. E. Hauser

Investigation: Hamed I. Albalawi, Zainab N. Khan, Ranim H. Rawas, Alexander U. Valle-Pérez, Sherin Abdelrahman

Methodology: Hamed I. Albalawi, Zainab N. Khan, Sherin Abdelrahman

Writing – original draft: Hamed I. Albalawi, Zainab N. Khan, Ranim H. Rawas, Alexander U. Valle-Pérez

Writing – review & editing: Zainab N. Khan, Hamed I. Albalawi, Charlotte A. E. Hauser

Ethics approval and consent to participate

Not applicable.

Consent for publication

Not applicable.

Availability of data

Data related to this work can be acquired by contacting the corresponding author with a reasonable justification.

References

1. Ngo TD, Kashani A, Imbalzano G, *et al.*, 2018, Additive manufacturing (3D printing): A review of materials, methods, applications and challenges. *Compos Part B Eng*, 143: 172–196.

https://doi.org/10.1016/j.compositesb.2018.02.012

2. Ford S, Minshall T, 2019, Invited review article: Where and how 3D printing is used in teaching and education. *Addit Manuf*, 25: 131–150.

https://doi.org/10.1016/j.addma.2018.10.028

3. Shahrubudin N, Lee TC, Ramlan R, 2019, An overview on 3D printing technology: Technological, materials, and applications. *Procedia Manuf*, 35: 1286–1296.

https://doi.org/10.1016/j.promfg.2019.06.089

4. Gao W, Zhang Y, Ramanujan D, *et al.*, 2015, The status, challenges, and future of additive manufacturing in engineering. *Comput Aided Des*, 69: 65–89.

https://doi.org/10.1016/j.cad.2015.04.001

5. Avila-Ramírez A, Valle-Pérez AU, Susapto HH, *et al.*, 2021, Ecologically friendly biofunctional ink for reconstruction of rigid living systems under wet conditions. *Int J Bioprint*, 7: 398.

https://doi.org/10.18063/ijb.v7i4.398

6. Albalawi HI, Khan ZN, Valle-Pérez AU, *et al.*, 2021, Sustainable and eco-friendly coral restoration through 3D printing and fabrication. *ACS Sustain. Chem Eng*, 9: 12634–12645.

https://doi.org/10.1021/acssuschemeng.1c04148

7. Wangpraseurt D, You S, Azam F, *et al.*, 2020, *et al.* Bionic 3D printed corals. *Nat Commun*, 11: 1748.

https://doi.org/10.1038/s41467-020-15486-4

8. Melchels FP, Domingos MA, Klein TJ, *et al.*, 2012, Additive manufacturing of tissues and organs. *Prog Polym Sci*, 37: 1079–1104.

https://doi.org/10.1016/j.progpolymsci.2011.11.007

9. Murphy SV, De Coppi P, Atala A, 2019, Opportunities and challenges of translational 3D bioprinting. *Nat Biomed Eng*, 4: 370–380.

https://doi.org/10.1038/s41551-019-0471-7

10. Ng WL, Lee JM, Zhou M, *et al.*, 2020, Vat polymerization-based bioprinting-process, materials, applications and regulatory challenges. *Biofabrication*, 12: 022001.

https://doi.org/10.1088/1758-5090/ab6034

11. Li W, Mille LS, Robledo JA, *et al.*, 2020, Recent advances in formulating and processing biomaterial inks for vat polymerization-based 3D printing. *Adv Healthc Mater*, 9: 2000156.

https://doi.org/10.1002/adhm.202000156

12. Elomaa L, Gerbeth L, Almalla A, *et al.*, 2023, Bioactive photocrosslinkable resin solely based on refined decellularized small intestine submucosa for vat photopolymerization of *in vitro* tissue mimics. *Addit Manuf*, 64: 103439.

https://doi.org/10.26434/chemrxiv-2022-f2hpc

13. Wang Y, Wang J, Ji Z, *et al.*, 2022, Application of bioprinting in ophthalmology. *Int J Bioprint*, 8: 552.

https://doi.org/10.18063/ijb.v8i2.552

14. Ozbolat IT, Hospodiuk M, 2016, Current advances and future perspectives in extrusion-based bioprinting. *Biomaterials*, 76: 321–343.

https://doi.org/10.1016/j.biomaterials.2015.10.076

15. Xing J, Luo X, Bermudez J, *et al.*, 2017, 3D Bioprinting of Scaffold Structure using Micro-Extrusion Technology. In: The Annual International Solid Freeform Fabrication Symposium, Austin.

https://doi.org/10.26153/16943

16. De León EH, Valle-Pérez AU, Khan ZN, *et al.*, 2023, Intelligent and smart biomaterials for sustainable 3D printing applications. *Curr Opin Biomed Eng*, 26: 100450.

https://doi.org/10.1016/j.cobme.2023.100450

17. Pradeep PV, Paul L, 2022, Review on novel biomaterials and innovative 3D printing techniques in biomedical applications. *Mater Today Proc.*, 58: 96–103.

https://doi.org/10.1016/j.matpr.2022.01.072

18. Xu H, Su Y, Liao Z, *et al.*, 2022, Coaxial bioprinting vascular constructs: A review. *Eur Polym J*, 179: 111549.

https://doi.org/10.1016/j.eurpolymj.2022.111549

19. Morgan FL, Moroni L, Baker MB, 2020, Dynamic bioinks to advance bioprinting. *Adv Healthc Mater*, 9: 1901798.

https://doi.org/10.1002/adhm.201901798

20. Colosi C, Shin SR, Manoharan V, *et al.*, 2016, Microfluidic bioprinting of heterogeneous 3D tissue constructs using low-viscosity bioink. *Adv Mater*, 28: 677–684.

https://doi.org/10.1002/adma.201503310

21. Khan ZN, Albalawi HI, Valle-Pérez AU, *et al.*, 2022, From 3D printed molds to bioprinted scaffolds: A hybrid material extrusion and vat polymerization bioprinting approach for soft matter constructs. *Mater Sci Addit Manuf*, 1: 7.

https://doi.org/10.18063/msam.v1i1.7

22. Abdelrahman S, Alsanie WF, Khan ZN, *et al.*, 2022, A Parkinson's disease model composed of 3D bioprinted dopaminergic neurons within a biomimetic peptide scaffold. *Biofabrication*, 14: 044103.

https://doi.org/10.1088/1758-5090/ac7eec

23. Skylar-Scott MA, Mueller J, Visser CW, *et al.*, 2019, Voxelated soft matter via multimaterial multinozzle 3D printing. *Nature*, 575: 330–335.

https://doi.org/10.1038/s41586-019-1736-8

24. Alrashoudi AA, Albalawi HI, Aldoukhi AH, *et al.*, 2021, Fabrication of a lateral flow assay for rapid in-field detection of COVID-19 antibodies using additive manufacturing printing technologies. *Int J Bioprint*, 7: 399.

https://doi.org/10.18063/ijb.v7i4.399

25. Khan Z, Kahin K, Rauf S, *et al.*, 2018, Optimization of a 3D bioprinting process using ultrashort peptide bioinks. *Int J Bioprint*, 5: 173.

https://doi.org/10.18063/ijb.v5i1.173

26. Susapto HH, Alhattab D, Abdelrahman S, *et al.*, 2021, Ultrashort peptide bioinks support automated printing of large-scale constructs assuring long-term survival of printed tissue constructs. *Nano Lett*, 21: 2719–2729.

https://doi.org/10.1021/acs.nanolett.0c04426

27. Kahin K, Khan Z, Albagami M, *et al.*, 2019, Development of a robotic 3D bioprinting and microfluidic pumping system for tissue and organ engineering. In: Gray BL, Becker H, editors. Microfluidics, BioMEMS, and Medical Microsystems XVII. 25 (SPIE, 2019).

https://doi.org/10.1117/12.2507237

28. Khan Z, Kahin K, Hauser C, 2021, Time-dependent pulsing of microfluidic pumps to enhance 3D bioprinting of peptide bioinks. In: Gray BL, Becker H, editors. Microfluidics, BioMEMS, and Medical Microsystems XIX, 5 (SPIE, 2021).

https://doi.org/10.1117/12.2578830